Available online at www.sciencedirect.com
SCIENCE DIRECT®
Journal of Sound and Vibration 275 (2004) 557–576
JOURNAL OF SOUND AND VIBRATION
www.elsevier.com/locate/jsvi

On the optimization of non-uniform acoustic liners on annular nozzles

L.M.B.C. Campos*, J.M.G.S. Oliveira

DEM-Secção de Mecânica Aerospacial, ISR, Instituto Superior Técnico, Av. Rovisco Pais, 1049-001 Lisboa Codex, Portugal

Received 21 October 2002; accepted 30 June 2003

Abstract

The solution of the convected wave equation, with uniform axial flow, in cylindrical co-ordinates, is used together with non-uniform impedance wall boundary conditions, to specify the acoustic modes in a cylindrical or annular nozzle. The radial eigenfunctions in this case are Bessel functions, and the method applies equally well to sheared and swirling mean flows, provided that the appropriate eigenfunctions are used. The eigenvalues or radial wavenumbers are determined by: (i) the roots of a linear combination of Bessel functions for a cylindrical nozzle with uniform wall impedance; (ii) the roots of a 2×2 determinant whose terms are linear combinations of Bessel and Neumann functions, for an annular nozzle with uniform but distinct impedances at each wall; (iii) the roots of an infinite determinant for a cylindrical nozzle with circumferentially non-uniform wall impedance; (iv) the roots of the determinant of a 2×2 block of infinite matrices for an annular nozzle with distinct, non-uniform impedance distributions at the two walls. The case of circumferentially non-uniform but axially uniform wall impedance, allows the existence of an axial wavenumber for each frequency and each eigenvalue or radial wavenumber. The acoustic liner may be optimized by maximizing the decay of a particular wave mode, e.g., the slowest decaying, or a combination of them, e.g., the total acoustic energy.

1. Introduction

Acoustic liners are widely used in jet engine inlet [1,2] and exhaust [3–10] ducts, as a passive means of noise reduction, in addition to mean flow effects [11–20]. The use of liners carries a weight penalty and may also adversely affect thrust and fuel consumption. The optimization of

*Corresponding author. Tel.: +351-21-847-09-42; fax: +351-21-841-75-39.
E-mail address: lmbcampos.aero@popsrv.ist.utl.pt (L.M.B.C. Campos).

0022-460X/$ - see front matter © 2003 Elsevier Ltd. All rights reserved.
doi:10.1016/j.jsv.2003.06.035

acoustic liners [21–23], gains additional freedom by the possibility of non-uniform impedance distribution [24–28]. In contrast with an uniform liner, the tailoring of the impedance distribution offers the prospect of greater acoustic attenuation for the same weight, or reduced weight for the same acoustic attenuation. The non-uniform liner may not be effective at low frequencies, for which passive attenuation is weak. It may not carry a significant advantage at high frequencies, which are readily absorbed by an uniform liner. The non-uniform liner should be most advantageous over the uniform liner at the intermediate frequencies, i.e., wavelengths of sound comparable to the scale of non-uniformity of the liner, for which the tailoring of the impedance distribution to the waveforms is most effective at attenuating them. These issues may be illustrated by considering a cylindrical duct with impedance varying circumferentially [29–32], axially or in both directions [33]. The case of circumferentially non-uniform impedance is used in the present paper to discuss the issues of optimization.

The need to consider non-uniformity of the impedance distribution on a scale comparable to the acoustic wavelength suggests that the acoustics of non-uniform liners is best studied via exact solutions of the acoustic wave equation, with the appropriate impedance wall boundary conditions. It can be easily seen that a non-uniform liner causes modal re-distribution, e.g., an isotropic mode $m = 0$ is modified by a circumferentially non-uniform liner into a non-isotropic mode, $m \neq 0$, which implies that the scattering effects generates harmonics $m = 1, 2, \ldots$. The effect of modal redistribution must be taken into account when assessing a non-uniform liner, since its effectiveness at absorbing a particular mode may be gained at the expense of reinforcing other modes. The non-uniform liner may be expected to change the natural modes of sound in a nozzle, e.g., of cylindrical or annular shape. The modelling of the acoustics of non-uniformly lined nozzles is similar in the absence of mean flow and in the presence of axial, shear [18–20] or swirling [34] flow, provided that the appropriate eigenfunctions are used. The latter are known to be Bessel functions in the case of a cylindrical nozzle with uniform axial flow. It should be borne in mind that vortical flows can absorb sound, in addition to the effect of the liner.

The starting point for our analysis is the solution of the convected wave equation (Section 2) for an uniform axial flow, in cylindrical co-ordinates (Section 2.1), applying to an annulus with dissimilar wall impedances (Section 2.2) or to a cylindrical nozzle with lined walls (Section 2.3). The case of non-uniform wall impedance varying circumferentially (Section 3) is considered both for the annular (Section 3.1) and for the cylindrical (Section 3.2) nozzles. The eigenvalues for the natural modes are specified by the roots of an infinite determinant in the cylindrical case, involving the Bessel eigenfunctions at the wall. In the case of an annular nozzle the Bessel and Neumann functions at the inner and outer walls lead to a four-block matrix, each block of infinite size, with the determinant of the whole matrix specifying the normal modes through its roots. The case of a cylindrical nozzle with uniform impedance is chosen to identify (Section 3.3) the mode with slowest axial decay. The wall liner is then made (Section 4) non-uniform, choosing the amplitude and phase of the first harmonic of the impedance distribution, to maximize the decay of the slowest decaying mode (Section 4.1). The accuracy of this optimization is checked, as concerns the decay rate of the mode (Section 4.2) and the optimal impedance distribution (Section 4.3). Other liner optimization strategies are discussed (Section 5).

2. Sound fields in a lined annular nozzle

The sound fields in a lined annular nozzle are determined by solving the convected wave equation in cylindrical co-ordinates with uniform axial flow (Section 2.1), and by applying boundary conditions at the inner and outer radius of the annulus, which may have distinct impedances (Section 2.2); these are taken to be uniform, including the particular case of a cylindrical nozzle (Section 2.3), before proceeding to circumferentially non-uniform liners.

2.1. Convected wave equation in cylindrical co-ordinates

The acoustic pressure p satisfies the convected [35,36] wave equation with sound speed c:

$$\left[(1/c^2)(\partial/\partial t + \mathbf{v}\cdot\boldsymbol{\nabla})^2 - \boldsymbol{\nabla}^2\right]p(\mathbf{x},t) = 0, \tag{1}$$

written in cylindrical co-ordinates $\mathbf{x} \equiv (r,\theta,z)$ in the case of a uniform axial flow of velocity $\mathbf{v} = U\mathbf{e}_z$:

$$\left[\frac{1}{c^2}\left(\frac{\partial}{\partial t} + U\frac{\partial}{\partial z}\right)^2 - \frac{1}{r}\frac{\partial}{\partial r}\left(r\frac{\partial}{\partial r}\right) - \frac{1}{r^2}\frac{\partial^2}{\partial\theta^2} - \frac{\partial^2}{\partial z^2}\right]p(r,\theta,z,t) = 0, \tag{2}$$

in an annulus (Fig. 1) of length L, so that

$$R \equiv r_2 \geqslant r \geqslant r_1 \equiv \sigma R, \quad 0 \leqslant z \leqslant L \equiv \mu R, \quad 0 \leqslant \theta < 2\pi, \tag{3a–c}$$

Here $\mu = L/R$ is the aspect ratio based on the outer radius, and the hollowness $\sigma = r_1/r_2$ is the inner radius as a fraction of the outer radius; for a cylindrical (hollow) nozzle, $r_1 = 0 = \sigma$, and for an annular nozzle $0 < \sigma < 1$. The impedance boundary condition [37] relates the Fourier time spectra of the acoustic pressure perturbation $\tilde{p}$ and acoustic velocity perturbation $\tilde{\mathbf{v}}$:

$$p(r,\theta,z,t) = \int_{-\infty}^{+\infty} \tilde{p}(r,\theta,z;\omega)\mathrm{e}^{-\mathrm{i}\omega t}\,\mathrm{d}\omega, \quad \mathbf{v}(r,\theta,z,t) = \int_{-\infty}^{+\infty} \tilde{\mathbf{v}}(r,\theta,z;\omega)\mathrm{e}^{-\mathrm{i}\omega t}\,\mathrm{d}\omega; \tag{4a, b}$$

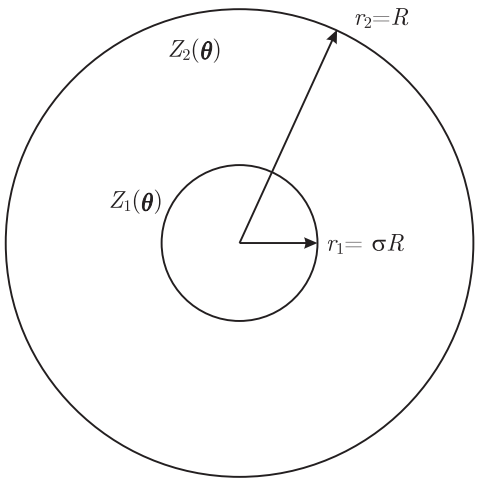

Fig. 1. Annular nozzle with circumferentially non-uniform impedance distributions $Z_1(\theta)$ over the inner surface of radius $r_1 = \sigma R$ with $0 < \sigma < 1$, and $Z_2(\theta)$ over the outer surface of radius $r_2 = R$.

the two walls may have distinct non-uniform wall impedances $\bar{Z}_s$:

$$s = 1, 2: \quad \tilde{p}(r_s, \theta, z; \omega) = \bar{Z}_s(\theta, z; \omega)\, \mathbf{n}_s \cdot \tilde{\mathbf{v}}(r_s, \theta, z; \omega), \tag{5a}$$

where $\tilde{\mathbf{v}}$ is the acoustic velocity perturbation spectrum and $\mathbf{n}_s$ is the unit vector normal to the wall, directed away from the fluid and towards the wall interior; $s = 1$ refers to the inner wall and $s = 2$ to the outer wall. In an annular cylindrical nozzle, $\mathbf{n}_1$ and $\mathbf{n}_2$ are radial vectors but $\mathbf{n}_1$ points to the axis whereas $\mathbf{n}_2$ points away from the axis. This can be taken into account writing

$$s = 1, 2: \quad \tilde{p}(r_s, \theta, z; \omega) = (-1)^s \bar{Z}_s(\theta, z; \omega)\, \tilde{v}_r(r_s, \theta, z; \omega); \tag{5b}$$

note that v_r is the radial component of the velocity perturbation $\mathbf{v}$ and is related to the acoustic pressure perturbation p by the linear radial component of the linearized momentum equation:

$$\rho(\partial/\partial t + U\partial/\partial z)v_r(r, \theta, z, t) + (\partial/\partial r)p(r, \theta, z, t) = 0, \tag{6}$$

where ρ denotes the mean flow mass density in (6).

Since the coefficients of wave equation (2) do not depend explicitly on (θ, z, t), it is convenient to use Fourier representations in these three variables, both for the acoustic pressure p and radial velocity v_r perturbations

$$p(r, \theta, z, t) = \sum_{m=-\infty}^{+\infty} \mathrm{e}^{\mathrm{i}m\theta} \int_{-\infty}^{+\infty} \mathrm{d}k\, \mathrm{e}^{\mathrm{i}kz} \int_{-\infty}^{+\infty} P_m(r; \omega, k)\, \mathrm{e}^{-\mathrm{i}\omega t}\, \mathrm{d}\omega, \tag{7a}$$

$$v_r(r, \theta, z, t) = \sum_{m=-\infty}^{+\infty} \mathrm{e}^{\mathrm{i}m\theta} \int_{-\infty}^{+\infty} \mathrm{d}k\, \mathrm{e}^{\mathrm{i}kz} \int_{-\infty}^{+\infty} V_m(r; \omega, k)\, \mathrm{e}^{-\mathrm{i}\omega t}\, \mathrm{d}\omega. \tag{7b}$$

viz.: (i) a Fourier series in the azimuthal direction (3c), with integer azimuthal wavenumber m; (ii) a Fourier integral in the axial direction (3b), with axial wavenumber k; (iii) a Fourier integral in time, involving the (m)-mode spectrum of the acoustic pressure P_m and radial velocity V_m, for a wave of frequency ω and axial wavenumber k at radius r. The radial dependence of the acoustic pressure spectrum is specified by substituting Eq. (7a) in Eq. (2), leading to [38,39] the Bessel equation

$$P \equiv P_m(r; \omega, k): \; r^2 P'' + rP' + (\kappa^2 r^2 - m^2)P = 0, \tag{8}$$

where the radial wavenumber is given by

$$\kappa^2 \equiv (\omega - kU)^2/c^2 - k^2. \tag{9}$$

The solution of Eq. (8) in an annulus is a linear combination of Bessel J_m and Neumann Y_m functions:

$$P_m(r; \omega, k) = A_m(\omega, k)\mathrm{J}_m(\kappa r) + B_m(\omega, k)\mathrm{Y}_m(\kappa r), \tag{10}$$

where the amplitudes A_m and B_m may depend on frequency and axial wavenumber and are determined by initial conditions and/or boundary conditions at the entry and exit from the duct.

2.2. Annular nozzle with dissimilar wall impedances

Substitution of the acoustic pressure (7a) and radial velocity (7b) perturbations in the radial component of the linearized momentum equation (6), leads to the polarization

relation

$$-\mathrm{i}\rho(\omega - kU)V_m(r;\omega,k) + (\mathrm{d}/\mathrm{d}r)P_m(r;\omega,k) = 0, \tag{11}$$

which may be applied at the walls (5b), with generally dissimilar impedances:

$$\mathrm{i}\left(\frac{\omega}{c} - kM\right)P_m(r;\omega,k) - (-1)^s Z_s(\mathrm{d}/\mathrm{d}r)P_m(r;\omega,k) = 0. \tag{12}$$

Two dimensionless parameters were introduced: the Mach number $M = U/c$, and the specific impedance, defined (13) as the ratio of the wall impedance to the impedance of a plane wave,

$$Z_s \equiv \bar{Z}_s/(\rho c). \tag{13}$$

Substitution of the radial eigenfunctions (10) in the boundary conditions (12) leads to

$$\begin{aligned} s = 1,2: \ \mathrm{i}\left(\frac{\omega}{c} - kM\right)&[A_m v\mathrm{J}_m(\kappa r_s) + B_m \mathrm{Y}_m(\kappa r_s)] \\ &- (-1)^s Z_s[A_m \kappa \mathrm{J}'_m(\kappa r_s) + B_m \kappa \mathrm{Y}'_m(\kappa r_s)] = 0, \end{aligned} \tag{14}$$

where prime denotes the derivative of the Bessel and Neumann functions with respect to their arguments.

Using the dimensionless parameter (15),

$$\alpha \equiv \omega/\kappa c - Mk/\kappa \tag{15}$$

and noting that $r_1 = \sigma R$, $r_2 = R$ the linear homogeneous system of Eq. (14), written in matrix form, is

$$\begin{bmatrix} \mathrm{i}\alpha \mathrm{J}_m(\kappa\sigma R) + Z_1 \mathrm{J}'_m(\kappa\sigma R) & \mathrm{i}\alpha \mathrm{Y}_m(\kappa\sigma R) + Z_1 \mathrm{Y}'_m(\kappa\sigma R) \\ \mathrm{i}\alpha \mathrm{J}_m(\kappa R) - Z_2 \mathrm{J}'_m(\kappa R) & \mathrm{i}\alpha \mathrm{Y}_m(\kappa R) - Z_2 \mathrm{Y}'_m(\kappa R) \end{bmatrix} \begin{bmatrix} A_m \\ B_m \end{bmatrix} = 0. \tag{16}$$

Since the amplitudes $A_m(\omega,k)$ and $B_m(\omega,k)$ cannot all vanish, the 2×2 determinant of the coefficients must vanish

$$\begin{aligned} 0 = D_0(k_{lmn}) \equiv &[\mathrm{i}\alpha \mathrm{J}_m(\kappa r_1) + Z_1 \mathrm{J}'_m(\kappa r_1)][\mathrm{i}\alpha \mathrm{Y}_m(\kappa r_2) - Z_2 \mathrm{Y}'_m(\kappa r_2)] \\ &- [\mathrm{i}\alpha \mathrm{J}_m(\kappa r_2) - Z_2 \mathrm{J}'_m(\kappa r_2)][\mathrm{i}\alpha \mathrm{Y}_m(\kappa r_1) + Z_1 \mathrm{Y}'_m(\kappa r_1)]. \end{aligned} \tag{17}$$

The vanishing of the 2×2 determinant of coefficients in Eq. (16) is the dispersion relation (17), whose roots are the radial wavenumbers κ_{lmn}, in the case of uniform, generally dissimilar wall impedances.

2.3. Cylindrical nozzle with uniform wall impedance

In a cylindrical nozzle (Fig. 2), the solution of Eq. (8) which is bounded at the origin is

$$P_m(r;\omega,k) = A_m(\omega,k)\mathrm{J}_m(\kappa r) \tag{18}$$

and simplifies the boundary condition (17) to

$$\mathrm{i}\alpha \mathrm{J}_m(\kappa R) - Z\mathrm{J}'_m(\kappa R) = 0. \tag{19}$$

The dimensionless frequency

$$\Omega \equiv \omega R/c, \tag{20}$$

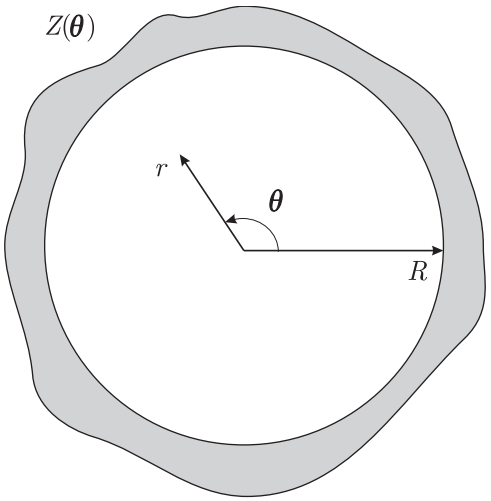

Fig. 2. In the particular case of the cylindrical nozzle of radius $r = R$ the circumferentially varying impedance distribution.

is related to the dimensionless axial and radial wavenumbers

$$\zeta = Rk, \quad \xi = R\kappa \tag{21}$$

by Eq. (9), viz.

$$\xi = \pm\sqrt{(\Omega - M\zeta)^2 - \zeta^2} \tag{22}$$

and appears in α in Eq. (15) as

$$\alpha = (\Omega - M\zeta)/\xi. \tag{23}$$

Substitution in the boundary condition (19) leads to

$$\mathrm{i}(\Omega - M\zeta)\,\mathrm{J}_m\left(\sqrt{(\Omega - M\zeta)^2 - \zeta^2}\right) - Z\sqrt{(\Omega - M\zeta)^2 - \zeta^2}\,\mathrm{J}'_m\left(\sqrt{(\Omega - M\zeta)^2 - \zeta^2}\right) = 0, \tag{24}$$

where the $(\pm)$ sign was dropped because of the parity of the Bessel functions of the first kind of integer order. If there is no flow, $M = 0$ and the boundary condition (24) simplifies to

$$\mathrm{i}\Omega\mathrm{J}_m\left(\sqrt{\Omega^2 - \zeta^2}\right) - Z\sqrt{\Omega^2 - \zeta^2}\,\mathrm{J}'_m\left(\sqrt{\Omega^2 - \zeta^2}\right) = 0. \tag{25}$$

Since this equation is even on ζ, it has symmetric solutions $\pm\zeta$. In terms of $\xi = \sqrt{\Omega^2 - \zeta^2}$, the boundary condition is written as

$$\mathrm{i}\Omega\mathrm{J}_m(\xi) - Z\xi\mathrm{J}'_m(\xi) = 0, \tag{26}$$

which is its simplest form.

3. Nozzle with circumferentially non-uniform wall impedance

The cases of one- and two-dimensional non-uniform wall distribution can be treated similarly, using single or double Fourier series, viz., one for each direction, for example, circumferential and axial. The case of circumferentially varying wall impedance is treated in detail for the annular nozzle with dissimilar wall impedances (Section 3.1), including the particular case of the cylindrical nozzle (Section 3.2). One notes that the distinction between cut-off (evanescent) and cut-on (propagating) modes, that exists for sound in a rigid walled nozzle, is not so clear in the case of an impedance wall, even when the impedance is uniform (Section 3.3).

3.1. Dissimilar inner and outer impedance distributions

The wall impedances at the inner $s=1$ and outer $s=2$ radius are represented by a Fourier series

$$s=1,2\text{: } Z_s(\theta)=\sum_{m'=-\infty}^{+\infty} Z_s^{m'}\,\mathrm{e}^{\mathrm{i}m'\theta} \tag{27}$$

with amplitudes $Z_s^{m'}$ of the harmonics m' of the impedance given by

$$Z_s^{m'}=\frac{1}{2\pi}\int_0^{2\pi} Z_s(\theta)e^{-\mathrm{i}m'\theta}\,\mathrm{d}\theta. \tag{28}$$

The Fourier representation (27), (28) applies to the wall impedance distributions which are functions of bounded variation, and thus allow discontinuous impedance distributions, e.g., ducts in which only some parts are lined. The impedance distributions may be different on the inner and outer walls, and they appear in the boundary conditions (5b). The equation of momentum (6) can be used to eliminate the radial acoustic velocity perturbation spectrum

$$r=r_s\text{: }\quad \frac{1}{c}\left(-\mathrm{i}\omega+U\frac{\partial}{\partial z}\right)\tilde{p}(r,\theta,z;\omega)+(-1)^s Z_s(\theta)\frac{\partial}{\partial r}\tilde{p}(r,\theta,z;\omega)=0. \tag{29}$$

The acoustic pressure is given both by Eqs. (4a) and (7a), leading to

$$\tilde{p}(r,\theta,z;\omega)=\sum_{m=-\infty}^{+\infty}\mathrm{e}^{\mathrm{i}m\theta}\int_{-\infty}^{+\infty}\mathrm{d}k\,\mathrm{e}^{\mathrm{i}kz}P_m(r;k,\omega) \tag{30}$$

with the radial eigenfunctions specified by Eq. (10)

$$\tilde{p}(r,\theta,z;\omega)=\sum_{m=-\infty}^{+\infty}\mathrm{e}^{\mathrm{i}m\theta}\int_{-\infty}^{+\infty}\mathrm{d}k\,\mathrm{e}^{\mathrm{i}kz}[A_m\mathrm{J}_m(\kappa r)+B_m\mathrm{Y}_m(\kappa r)], \tag{31}$$

as a superposition of azimuthal and axial harmonics, with wavenumbers, respectively, m,k, related to frequency ω and radial wavenumber κ by Eq. (9).

Substitution of the decomposition into harmonics (m,k) of the acoustic pressure (31) and harmonics m' of the wall impedances (27) into the boundary conditions

(29) yields

$$0 = \mathrm{i}\frac{\omega - Uk}{c} \sum_{m=-\infty}^{+\infty} \mathrm{e}^{\mathrm{i}m\theta}[A_m(\omega,k)\mathrm{J}_m(\kappa r_s) + B_m(\omega,k)\mathrm{Y}_m(\kappa r_s)]$$
$$- (-1)^s \sum_{m,m'=-\infty}^{+\infty} \mathrm{e}^{\mathrm{i}(m+m')\theta} Z_s^{m'} \kappa [A_m(\omega,k)\mathrm{J}'_m(\kappa r_s) + B_m(\omega,k)\mathrm{Y}'_m(\kappa r_s)]. \tag{32}$$

Use of Eqs. (9) and (15) simplifies these two boundary conditions to

$$\sum_{m=-\infty}^{+\infty} \mathrm{e}^{\mathrm{i}m\theta} \left\{ \mathrm{i}\alpha[A_m \mathrm{J}_m(\kappa r_s) + B_m \mathrm{Y}_m(\kappa r_s)] \right.$$
$$\left. - (-1)^s \sum_{m'=-\infty}^{+\infty} Z_s^{m-m'} [A_{m'} \mathrm{J}'_{m'}(\kappa r_s) + B_{m'} \mathrm{Y}'_{m'}(\kappa r_s)] \right\} = 0, \tag{33}$$

where, in the second term, $m + m'$ was replaced by m', and then m exchanged with m'. Since each of the terms in curly brackets must vanish, introducing the identity matrix $\delta_{mm'}$ leads to the linear homogeneous system of equations

$$\sum_{m'=-\infty}^{+\infty} [\mathrm{i}\alpha \mathrm{J}_{m'}(\kappa r_s)\delta_{mm'} - (-1)^s Z_s^{m-m'} \mathrm{J}'_{m'}(\kappa r_s)] A_{m'}(\omega,k)$$
$$+ \sum_{m'=-\infty}^{+\infty} [\mathrm{i}\alpha \mathrm{Y}_{m'}(\kappa r_s)\delta_{mm'} - (-1)^s Z_s^{m-m'} \mathrm{Y}'_{m'}(\kappa r_s)] B_{m'}(\omega,k) = 0. \tag{34}$$

Since the amplitudes $A_{m'}$ and $B_{m'}$ cannot be all zero, the determinant of coefficients must vanish:

$$0 = D(k_{mn}) = \begin{vmatrix} \mathrm{i}\alpha \mathrm{J}_m(\kappa r_1)\delta_{mm'} + Z_1^{m'-m} \mathrm{J}'_m(\kappa r_1) & \mathrm{i}\alpha \mathrm{Y}_m(\kappa r_1)\delta_{mm'} + Z_1^{m'-m} \mathrm{Y}'_m(\kappa r_1) \\ \mathrm{i}\alpha \mathrm{J}_m(\kappa r_2)\delta_{mm'} - Z_2^{m'-m} \mathrm{J}'_m(\kappa r_2) & \mathrm{i}\alpha \mathrm{Y}_m(\kappa r_2)\delta_{mm'} - Z_2^{m'-m} \mathrm{Y}'_m(\kappa r_2) \end{vmatrix}. \tag{35}$$

This is a 2×2 determinant, of which each of the four terms is an infinite determinant $m, m' = 0, \pm 1, \ldots, \pm\infty$; its roots specify the radial wavenumbers κ_{mn} or axial wavenumbers k_{mn}, and hence the decay of the modes.

3.2. Cylindrical nozzle with circumferentially varying wall impedance

A particular case $r_1 = 0$ is the cylindrical nozzle of radius R with a specific wall impedance $Z(\theta)$ given by

$$Z(\theta) = \sum_{m'=-\infty}^{+\infty} Z_{m'} \mathrm{e}^{\mathrm{i}m'\theta} \tag{36}$$

with coefficients of harmonics

$$Z_{m'} = \frac{1}{2\pi} \int_0^{2\pi} Z(\theta) \mathrm{e}^{-\mathrm{i}m'\theta} \, \mathrm{d}\theta. \tag{37}$$

This case is obtained by setting the coefficients B_m to zero in Eq. (10) and omitting the boundary condition at the inner wall. Eq. (34) reduces to the first term, where m and m'

can be interchanged:

$$\sum_{m=-\infty}^{+\infty} [\mathrm{i}\alpha \mathrm{J}_m(\kappa R)\delta_{mm'} - Z_{m'-m}\mathrm{J}'_m(\kappa R)]A_m(\omega, k) = 0. \tag{38}$$

This is an infinite system of equations (one for each value of m') and, since not all A_m vanish, the determinant must vanish:

$$D(k_n) = \det N_{m'm} = 0, \tag{39}$$

where the matrix $N_{m'm}$ is given by

$$N_{m'm} = \mathrm{i}\alpha \mathrm{J}_m(\kappa R)\delta_{m'm} - Z_{m'-m}\mathrm{J}'_m(\kappa R). \tag{40}$$

The roots of Eq. (39) specify the radial wavenumbers κ_n, and, through Eq. (9), the axial wavenumbers k_n for a given frequency.

Using α in Eq. (23), determinant (39) can be written, centred on element N_{mm}, as

$$\begin{aligned} D(k_n) &= \begin{vmatrix} \mathrm{i}\dfrac{\Omega - M\zeta}{\xi}\mathrm{J}_{m-1}(\xi) - Z_0\mathrm{J}'_{m-1}(\xi) & -Z_{-1}\mathrm{J}'_m(\xi) & -Z_{-2}\mathrm{J}'_{m+1}(\xi) \\ -Z_{+1}\mathrm{J}'_{m-1}(\xi) & \mathrm{i}\dfrac{\Omega - M\zeta}{\xi}\mathrm{J}_m(\xi) - Z_0\mathrm{J}'_m(\xi) & -Z_{-1}\mathrm{J}'_{m+1}(\xi) \\ -Z_{+2}\mathrm{J}'_{m-1}(\xi) & -Z_{+1}\mathrm{J}'_m(\xi) & \mathrm{i}\dfrac{\Omega - M\zeta}{\xi}\mathrm{J}_{m+1}(\xi) - Z_0\mathrm{J}'_{m+1}(\xi) \end{vmatrix} \\ &= 0, \end{aligned} \tag{41}$$

where only the central 3×3 part is written explicitly. To find the roots of the determinant, ξ is expressed in terms of ζ using Eq. (22), where the $\pm$ sign can be dropped:

$$\xi = \sqrt{(\Omega - \zeta M)^2 - \zeta^2}, \tag{42}$$

because when the sign of ξ is reversed, the signs of the terms of rows with m odd in determinant Eq. (41) are reversed, and thus the roots of the determinant remain the same.

When there is no mean flow inside the duct, $M = 0$ and Eq. (41) can be simplified to

$$\begin{aligned} D(\kappa_n) &= \begin{vmatrix} \mathrm{i}(\Omega/\xi)\mathrm{J}_{m-1}(\xi) - Z_0\mathrm{J}'_{m-1}(\xi) & -Z_{-1}\mathrm{J}'_m(\xi) & -Z_{-2}\mathrm{J}'_{m+1}(\xi) \\ -Z_{+1}\mathrm{J}'_{m-1}(\xi) & \mathrm{i}(\Omega/\xi)\mathrm{J}_m(\xi) - Z_0\mathrm{J}'_m(\xi) & -Z_{-1}\mathrm{J}'_{m+1}(\xi) \\ -Z_{+2}\mathrm{J}'_{m-1}(\xi) & -Z_{+1}\mathrm{J}'_m(\xi) & \mathrm{i}(\Omega/\xi)\mathrm{J}_{m+1}(\xi) - Z_0\mathrm{J}'_{m+1}(\xi) \end{vmatrix} \\ &= 0. \end{aligned} \tag{43}$$

In this case the determinant depends only on ξ and Ω and its roots specify the axial wavenumber through

$$\zeta = \pm\sqrt{\Omega^2 - \xi^2}. \tag{44}$$

In the presence of mean flow $M \neq 0$, the roots ξ of Eq. (41) specify the axial wavenumber ζ by solving Eq. (42), viz.,

$$(1 - M^2)\zeta = -\Omega M \pm \sqrt{\Omega^2 - (1 - M^2)\xi^2}, \tag{45}$$

which simplifies to Eq. (44) for $M = 0$.

3.3. Fundamental longitudinal mode with uniform impedance

In the case of a rigid wall, the boundary condition (5a) is replaced by zero normal velocity $v_r = 0$, or zero normal gradient of the acoustic pressure $\partial p/\partial r = 0$, corresponding to infinite impedance $Z = \infty$ in Eq. (25). In this case the radial wavenumbers are the roots of $\mathrm{J}'_m(\xi) = 0$ in Eq. (26). Thus, if j_{mn} denote the roots of the derivative of the Bessel function J_m, the radial wavenumbers are real:

$$\mathrm{J}'_m(j_{mn}) = 0 \quad \Rightarrow \quad \kappa_{mn} = j_{mn}/R. \tag{46}$$

The corresponding axial wavenumbers

$$k_{mn} = \sqrt{(\omega/c)^2 - (j_{mn}/R)^2} \tag{47}$$

are: (i) real for propagating or cut-on modes if $\omega R/c > |j_{mn}|$, i.e., for the lowest order modes; (ii) for sufficiently high radial order n, such that $|j_{mn}| > \omega R/c$ the modes are imaginary, i.e., cut-off or evanescent.

For impedance wall condition, even in the case of uniform impedance (19), the radial wavenumber κ_{mn} is generally complex, and even in the absence of mean flow, the axial wavenumber k_{mn} is also complex (9):

$$k_{mn} = \sqrt{(\omega/c)^2 - \kappa_{mn}^2} \tag{48}$$

and the preceding distinction is not so clear. The real part of the axial wavenumber specifies the periodicity of the acoustic field along the axis of the duct; whereas the imaginary part specifies its decay:

$$\exp(\mathrm{i}k_{mn}z) = \exp[\mathrm{i}z\,\mathrm{Re}(k_{mn})]\exp[-z\,\mathrm{Im}(k_{mn})]. \tag{49}$$

One considers as an example a cylindrical nozzle of radius $R = 1$ m without mean flow $U = 0$, for the circumferential mode $m = 14$, which could be generated by a compressor or turbine stage with $m/2 = 7$ blades. The dimensionless axial wavenumber ζ is plotted versus dimensionless frequency Ω in Fig. 3, which shows the first 10 modes, for a specific impedance

$$Z_0 \equiv \bar{Z}_0/\rho c = 2.5 - \mathrm{i}0.4. \tag{50}$$

Generally, impedance (5a) is a function of frequency, and would have different values for distinct modes. In Fig. 3 and subsequent figures the same impedance is considered for all modes, in order to make more clear the modal interaction associated with non-uniform impedance. It is clear that higher order n modes, for a fixed frequency Ω, decay faster, i.e., have larger $\mathrm{Im}(\zeta_n)$. For each order n, as the frequency increases, the imaginary part reduces, but the transition is not abrupt, i.e., there is no abrupt jump from cut-off to cut-on modes. The slowest decaying mode ζ_1 with uniform

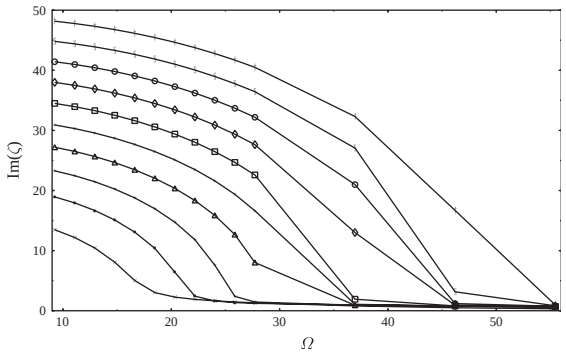

Fig. 3. Imaginary part of first 10 $n = 1, \ldots, 10$ dimensionless axial wavenumbers $\zeta = kR$ as a function of dimensionless frequency $\Omega = \omega R/c$, for a cylindrical nozzle without mean flow, with uniform wall impedance (50). Key for axial wavenumbers: $-\times-$, 1; $-\bullet-$, 2; $-\bigstar-$, 3; $-\triangle-$, 4; $-*-$, 5; $-\square-$, 6; $-\diamond-$, 7; -○-, 8; -§ -, 9; -†-, 10.

impedance Z_0, is considered next, in order to optimize the impedance distribution $Z(\theta)$ to maximize the decay of acoustic pressure.

4. Maximization of the axial decay of the acoustic field

The effect of a circumferentially non-uniform acoustic liner on a cylindrical nozzle is exemplified (Section 4.1) by showing how the axial wavenumber varies with the amplitude of the first harmonic of the impedance, to maximize its imaginary part or spatial decay. This specifies the optimum impedance distribution, with an accuracy which can be estimated by performing the calculations in several alternative ways (Section 4.2). Using these methods it is possible to implement a liner optimization strategy (Section 4.3), which selects the modes with slowest axial decay and maximizes their axial decay by selecting the non-uniform impedance distribution.

4.1. Impedance distribution for the fastest acoustic decay

A possible optimization criterion for a circumferentially non-uniform acoustic liner is to maximize the imaginary part of the axial wavenumber for the most significant modes. This can be illustrated by changing the circumferential liner impedance to maximize the imaginary part of the axial wavenumber of the slowest decaying mode ζ_1, calculated above for an uniform liner. The baseline case is taken to be a wave of frequency $f = 1$ kHz in a cylindrical nozzle of radius $R = 1$ m, so that the dimensionless frequency is $\Omega = \omega R/c = 2\pi f R/c = 18.48$ for a sound speed $c = 340$ m/s. The roots of Eq. (26) specify the dimensionless radial wavenumber ξ_n and hence by Eq. (44), the dimensionless axial wavenumber ζ_n. The root leading to the smallest imaginary part of $\zeta_n = k_n/R$, and hence Eq. (49) the slowest decay, is

$$\zeta_1 = 8.03438 + \mathrm{i}3.020068. \tag{51}$$

The imaginary part should be maximized next by optimizing the circumferential impedance distribution. The impedance distribution is made circumferentially non-uniform by adding to Z_0

the first terms of the Fourier series (36), viz.:

$$Z(\theta) = Z_0 + Z_1 \mathrm{e}^{\mathrm{i}\theta} + Z_{-1}\mathrm{e}^{-\mathrm{i}\theta}, \tag{52}$$

choosing the combination

$$Z_1 = Z_{-1} = \varepsilon Z_0, \tag{53}$$

so that it takes the form

$$Z(\theta) = Z_0(1 + \varepsilon \cos\theta). \tag{54}$$

The complex impedance correction can be chosen at will, provided that $\mathrm{Re}[Z(\theta)] > 0$ for all θ, viz., $\mathrm{Re}(\varepsilon) > -1$; this will be satisfied by taking $|\varepsilon| < 1$, i.e., an impedance correction smaller than the baseline value.

In the no-flow case ($M = 0$) the dimensionless wavenumbers ξ are given by the roots of determinant (43). For computational purposes it can be truncated to a 3×3 determinant centred on the $m = 14$ element. The axial dimensionless wavenumber ζ can then be determined by use of Eq. (44). The roots $D = 0$ of Eq. (43) are determined as follows. First, the values of D are calculated on a grid, then the points where $\mathrm{Re}(D)$ change sign and where $\mathrm{Im}(D)$ change sign are determined. The intersection of both sets of points gives approximated values of the roots, which are then used to determine more precise values using the secant method. The radial and axial wavenumbers were determined for

$$0 \leqslant \mathrm{Re}\,(\varepsilon) \leqslant 1, \quad -1 \leqslant \mathrm{Im}\,(\varepsilon) \leqslant 1. \tag{55}$$

In the present case, where only the first terms of the Fourier series (36) are used, the determinant D depends only on ε^2:

$$D(\kappa_n) = \begin{vmatrix} \mathrm{i}(\Omega/\xi)\mathrm{J}_{m-1}(\xi) - Z_0\mathrm{J}'_{m-1}(\xi) & -\varepsilon Z_0 \mathrm{J}'_m(\xi) & 0 \\ -\varepsilon Z_0 \mathrm{J}'_{m-1}(\xi) & \mathrm{i}(\Omega/\xi)\mathrm{J}_m(\xi) - Z_0\mathrm{J}'_m(\xi) & -\varepsilon Z_0 \mathrm{J}'_{m+1}(\xi) \\ 0 & -\varepsilon Z_0 \mathrm{J}'_m(\xi) & \mathrm{i}(\Omega/\xi)\mathrm{J}_{m+1}(\xi) - Z_0\mathrm{J}'_{m+1}(\xi) \end{vmatrix} = 0. \tag{56}$$

Therefore there is no need to determine the wavenumbers for negative values of $\mathrm{Re}(\varepsilon)$. In Fig. 4 the axial wavenumbers determined are presented for representative values of $\mathrm{Re}(\varepsilon)$. For small values of $\mathrm{Re}(\varepsilon)$ and $\mathrm{Im}(\varepsilon)$ —typically $|\mathrm{Re}(\varepsilon)| \leqslant 0.2$ and $|\mathrm{Im}(\varepsilon)| \leqslant 0.4$—changes in wavenumber due to the non-uniformity are small enough to clearly identify each wavenumber with a definite value of m. In this range it is possible to find values of ε that maximize the imaginary part of the dimensionless axial wavenumber ζ and thus the mode decay. As ε increases, mode coupling strengthens and change in ζ increases. It is no longer possible to clearly assign each wavenumber obtained using the 3×3 determinant for a single value of m. Therefore, for large values of ε, mode mixing due to the non-uniform wall impedance makes impossible a one-to-one correspondence with the modes in a nozzle with rigid walls or uniform wall impedance.

4.2. Truncation of determinant and accuracy of optimization

The results of the previous section were obtained by determining the roots of the infinite determinant (56) truncated to a 3×3 determinant. To understand how this affects the results, the

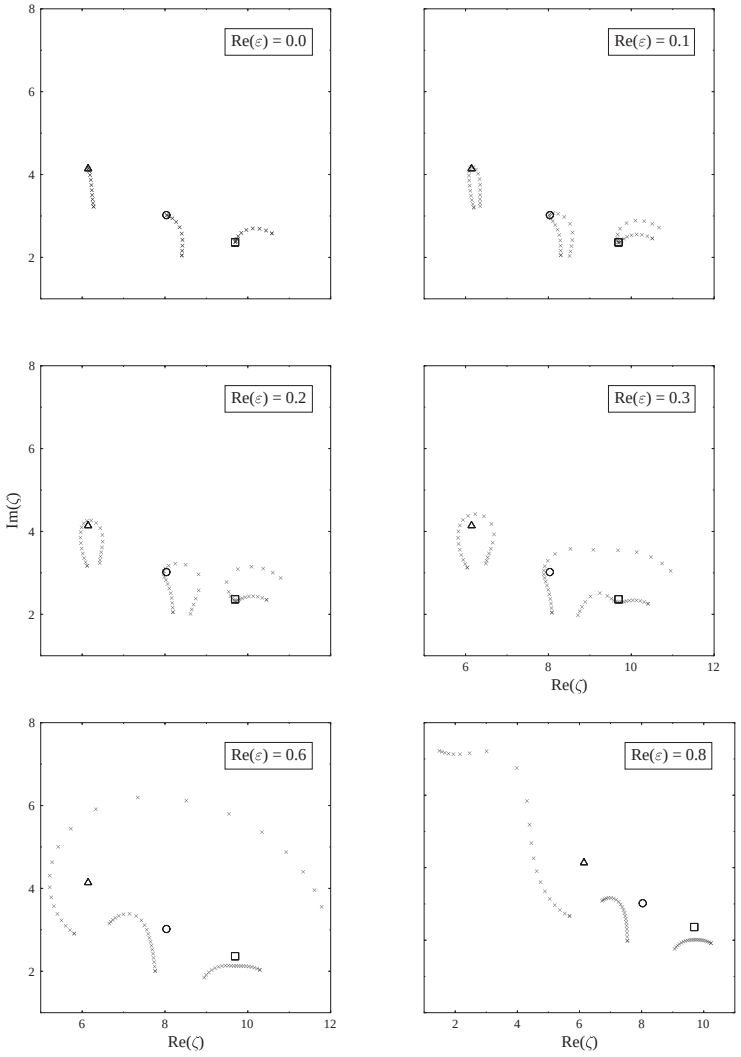

Fig. 4. Dimensionless axial wavenumbers $\zeta = kR$ for a cylindrical nozzle without mean flow, and with circumferentially non-uniform wall impedance. In each plot $\mathrm{Re}(\varepsilon)$ is kept constant and $\mathrm{Im}(\varepsilon)$ varies from -1 to 1, in steps of 0.1. For comparison, the wavenumbers obtained with uniform impedance for $m = 13$ (□), $m = 14$ (○) and $m = 15$ (△) are also represented.

eigenvalues were determined for uniform impedance and, for a few values of ε, for 2×2, 3×3, 4×4 and 5×5 determinants. The values of ε were chosen small enough that the radial eigenvalues could by assigned to $m = 14$. The radial eigenvalues obtained, presented in Table 1, show that the difference in the results obtained with determinants 3×3, 4×4 and 5×5 is small. Truncation to 3×3 determinant is therefore possible without serious loss of accuracy. Table 1 also shows that the accuracy of the results from 3×3 determinant tend to reduce as ε increases. This is to be expected, since, when going from a $n \times n$ determinant to a $(n+1) \times (n+1)$ the additional term that appears is proportional to ε^2. Therefore, the smaller the value of the correction, the better the accuracy obtained with a 3×3 determinant.

Table 1
Dimensionless radial eigenvalues determined using determinant (56) truncated in several different ways, for four different values of non-uniform impedance correction ε in Eq. (54), for a cylindrical nozzle without mean flow, with uniform baseline wall impedance (50)

Determinant	$\varepsilon = 0.1 + 0.1\mathrm{i}$	$\varepsilon = 0.1 + 0.2\mathrm{i}$	$\varepsilon = 0.2 + 0.1\mathrm{i}$	$\varepsilon = 0.2 + 0.2\mathrm{i}$
Uniform impedance	$16.9741 - 1.4295\mathrm{i}$	$16.9741 - 1.4295\mathrm{i}$	$16.9741 - 1.4295\mathrm{i}$	$16.9741 - 1.4295\mathrm{i}$
2×2 $(m = 13, 14)$	$16.9833 - 1.4128\mathrm{i}$	$16.9686 - 1.3831\mathrm{i}$	$17.0165 - 1.4090\mathrm{i}$	$17.0087 - 1.3654\mathrm{i}$
2×2 $(m = 14, 15)$	$16.9634 - 1.4286\mathrm{i}$	$16.9509 - 1.4429\mathrm{i}$	$16.9546 - 1.4124\mathrm{i}$	$16.9334 - 1.4246\mathrm{i}$
3×3 $(m = 13–15)$	$16.9729 - 1.4123\mathrm{i}$	$16.9481 - 1.3960\mathrm{i}$	$16.9953 - 1.3940\mathrm{i}$	$16.9712 - 1.3662\mathrm{i}$
4×4 $(m = 12–15)$	$16.9725 - 1.4121\mathrm{i}$	$16.9467 - 1.3978\mathrm{i}$	$16.9951 - 1.3918\mathrm{i}$	$16.9663 - 1.3646\mathrm{i}$
4×4 $(m = 13–16)$	$16.9729 - 1.4122\mathrm{i}$	$16.9478 - 1.3959\mathrm{i}$	$16.9956 - 1.3939\mathrm{i}$	$16.9711 - 1.3654\mathrm{i}$
5×5 $(m = 12–16)$	$16.9725 - 1.4121\mathrm{i}$	$16.9464 - 1.3977\mathrm{i}$	$16.9954 - 1.3917\mathrm{i}$	$16.9662 - 1.3639\mathrm{i}$

Table 2
Dimensionless radial eigenvalues determined using determinant (56) truncated in several different ways, for non-uniform impedance $\varepsilon = 0.7 + 0.6\mathrm{i}$ in Eq. (54), applied to a cylindrical nozzle without mean flow, with uniform baseline wall impedance (50)

Determinant	$\varepsilon = 0.7 + 0.6\mathrm{i}$
2×2 $(m = 13, 14)$	$17.2087 - 0.96035\mathrm{i}$
2×2 $(m = 14, 15)$	$16.7119 - 1.30537\mathrm{i}$
3×3 $(m = 13–15)$	$17.0455 - 1.07537\mathrm{i}$
4×4 $(m = 12–15)$	$16.8800 - 0.97081\mathrm{i}$
4×4 $(m = 13–16)$	$17.0323 - 1.05448\mathrm{i}$
5×5 $(m = 12–16)$	$16.8800 - 0.95862\mathrm{i}$

A large value of ε leads to a strong coupling between the modes. Therefore, it would be expected that the roots of the truncated determinant vary much more. Larger determinants include more modes that will couple with the modes already included in smaller determinants and change its values significantly. This is apparent in Table 2, where radial eigenvalues determined for $\varepsilon = 0.7 + 0.6\mathrm{i}$ are presented. The real part vary by a few percent and the imaginary part vary by more than 20%. The conclusion is that truncation of the infinite determinant (56) to a 3×3 determinant is reliable for small values of ε, in the range of $|\mathrm{Re}(\varepsilon)| \leqslant 0.2$ and $|\mathrm{Im}(\varepsilon)| \leqslant 0.4$, when mode coupling is weak, as seen on (Section 4.1); and that truncation into a small determinant is unreliable for values of ε outside that range, because of strong mode coupling; in this case truncation may still be possible, but to a larger size of determinant.

4.3. Optimization strategy for non-uniform liner

Having discussed the effect of the non-uniform liner on the acoustic modes (Section 4.1), and the accuracy of the calculations (Section 4.2), an example of the implementation of the optimization strategy is given. The starting point is the set of dimensionless radial wavenumbers ξ, which are given by the roots of the infinite determinant (56). These specify through Eq. (45) the

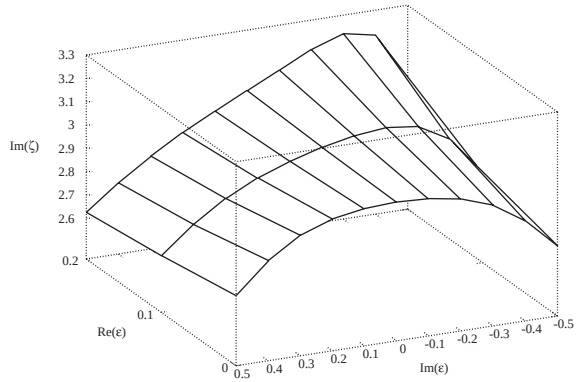

Fig. 5. The zero of $D(\xi) = 0$ for which the spatial decay $\mathrm{Im}(\zeta)$ is slowest is plotted as a function of the real $\mathrm{Re}(\varepsilon)$ and imaginary $\mathrm{Im}(\varepsilon)$ parts of the impedance correction, based on the 3×3 determinant centred on mode $m = 14$.

eigenvalues of the axial dimensionless wavenumber ζ, which will differ from case (46) of uniform impedance ζ_0. When the impedance perturbation is not large, it is in general possible to identify the eigenvalue closest to, or corresponding to ζ_0, which is denoted ζ. The mode with the slowest axial decay (51) is $\zeta_1 = 8.03438 + \mathrm{i}3.020068$. The optimization strategy is to select the complex amplitude ε of the first harmonic of the impedance distribution (54), so as to maximize the imaginary part of Eq. (51), and achieve the fastest axial decay.

The imaginary part of ζ, which specifies the axial decay, is plotted versus the real and imaginary part of the impedance perturbation ε in Fig. 5, using a 3×3 determinant (56) centred on mode $m = 14$. The maximum value of the imaginary part of the dimensionless axial wavenumber is

$$\mathrm{Im}(\zeta_1) = \mathrm{Im}(kR) = 3.220793 \tag{57}$$

and occurs for an impedance correction

$$\varepsilon = 0.2 - \mathrm{i}0.3, \tag{58}$$

leading in Eqs. (52) and (54) to a final impedance

$$Z(\theta) = 2.5 - \mathrm{i}0.4 + \cos\theta(0.38 - 0.83\mathrm{i}) \tag{59}$$

as a continuous function of azimuthal angle θ, which could be approximated by uniform splices.

5. Discussion

The preceding optimization method could be refined in several ways e.g., by (i) considering more parameters in the non-uniform impedance distribution and by (ii) using more elaborate optimization criteria. Concerning (i), additional terms in the Fourier series (36) could be considered beyond (52)–(54), e.g., for an even wall impedance distribution

$$Z(\theta) = Z_0 \left[1 + \sum_{n=1}^{\infty} \varepsilon_n \cos(n\theta) \right], \tag{60}$$

where besides the optimization with regard to $\varepsilon_1 \equiv \varepsilon$, there could be optimization with regard to ε_n:

$$\varepsilon_n = Z_n/Z_0 = Z_{-n}/Z_0, \tag{61}$$

up to a sufficient order to tailor precisely the circumferential distribution of impedance $Z(\theta)$. Note that if the circumferential impedance distribution $Z(\theta)$ is a function with continuous derivative for $0 \leqslant \theta < 2\pi$, i.e., $Z \in \mathscr{C}^1(0, 2\pi)$, then coefficients (37) are $O(1/(m')^2)$, and the Fourier series (36) converges absolutely and uniformly in the usual sense:

$$C0\text{: } Z(\theta) = \lim_{M \to \infty} \sum_{m'=-M}^{+M} Z_{m'} \, \mathrm{e}^{\mathrm{i}m'\theta}. \tag{62}$$

The case of discontinuous impedance distribution is important, since it corresponds to a nozzle lined by impedance patches. In this case [40] coefficients (37) are $O(1/m')$ and the Fourier series (36) converges non-uniformly in the usual sense (62). The non-uniformity of convergence at the points of discontinuity leads to the Gibbs phenomenon, which can be explained as (i) at a point of discontinuity $\theta = \theta_0$ of the impedance $Z(\theta)$, the Fourier series converges [41] to the mean of the right and left values $[Z(\theta_0 + 0) + Z(\theta_0 - 0)]/2$; (ii) since series (62) is a continuous function, it cannot follow the jump of the impedance from $Z(\theta_0 - 0)$ to $Z(\theta_0 + 0) \neq Z(\theta_0 - 0)$, and thus it oscillates on either side of the discontinuity. Adding more terms to the Fourier series does not eliminate the oscillations near the discontinuity, it just confines them to a narrower interval in the neighbourhood of the discontinuity. These spurious oscillations can be interpreted [43,44] as sources localized at the points of discontinuity; the non-uniform convergence of the series at the points of discontinuity may give the appearance of non-uniqueness of the solution when computational methods are used since the sum of the series may change when the order of the terms are altered. The problem of non-uniform convergence of the Fourier series (36) for a discontinuous impedance, when coefficients (37) are $O(1/m')$, can be overcome [41] replacing the usual method $C0$ of summation of series (62) by the Cèsaro $C1$ sum:

$$C1\text{: } Z(\theta) = \lim_{M \to \infty} \sum_{m'=-M}^{+M} \left(1 - \frac{m'}{M}\right) Z_{m'} \mathrm{e}^{\mathrm{i}m'\theta}. \tag{63}$$

It can be shown [41] that: (i) when the Fourier series Eq. (36) converges $C0$ as in Eq. (62), it also converges $C1$ as in Eq. (63) to the same sum, e.g., for an impedance distribution with continuous first derivative; (ii) in the case of a discontinuous impedance distribution of bounded variation, when the $C0$ sum (62) converges non-uniformly, the $C1$ sum (63) converges uniformly.

The preceding aspect of the representation of a discontinuous impedance distribution by a conditionally continuous Fourier series was a purely mathematical issue; a more fundamental physical consideration arises in connection with discontinuous impedance distributions. At the point of discontinuity, the boundary condition (12) does not apply; this point is a singularity, where a wave source could be located. This possibility is excluded by applying an additional condition, e.g., integrability of the wave field in the neighbourhood of the discontinuity [42]. An additional issue arises concerning the convergence of the two infinite series, or the accuracy of the two truncated series associated with the problem, viz.: (i) N terms for the series of eigenfunctions (31) representing the wave field; (ii) M terms for the Fourier series (27) representing the wall

impedance. Convergence may fail, and accuracy will be poor, if: (i) N is kept fixed and M increased, because of inadequate representation of the wave field; (ii) M is kept fixed and N increased, because of poor representation of the wall impedance. Convergence requires a suitable ratio M/N, to ensure good matching of the wave field and wall impedance; a good choice of M/N can lead to satisfactory accuracy with a moderate number of terms [43,44]. This question arises not only for discontinuous wall impedance, but also for changes in cross-section or perforated diaphragms, when matching acoustic ducts [42] or electromagnetic waveguides [43–45]. This issue arises, for example, in connection with the step wall impedance distribution in the one-dimensional problem dealt with in Ref. [28]. It does not arise in examples (52) of the present three-dimensional problem, which use continuous wall impedance distributions.

The optimization criterion could be the spatial decay of the acoustic energy for a superposition of modes

$$E_m(z) = \sum_n E_{nm} \mathrm{e}^{-2z\ \mathrm{Im}(k_{nm})}, \tag{64}$$

instead of just one. The energy E_{nm} of each mode would be equal in the case of equipartition $E_{nm} = E_{m0}$, or it could be determined for each mode by considering the problem of sound generation in a non-uniformly lined duct. In these more elaborate implementations, the method of optimization of acoustic liners would still retain the same basic features demonstrated before. In the choice of liner optimization strategies it is important to take into account the issue of mode identification or classification. The widely used distinction between cut-off (evanescent) modes with imaginary axial wavenumber and cut-on (propagating) modes with real axial wavenumbers applies clearly to a nozzle with a rigid wall. In the case of a nozzle with a uniform wall impedance, for a real frequency, the axial wavenumbers will have an imaginary part, specifying their spatial decay, but they can still be traced back to the modes of a rigid walled nozzle, for each circumferential wavenumber m. A circumferentially non-uniform wall impedance couples different m modes, and if it is sufficiently non-uniform the modes become mixed (see Fig. 4), and can no longer be traced back to the cut-on or cut-off modes of a rigid walled nozzle. Thus, for a strongly non-uniform liner, the minimization of the total acoustic energy remains a feasible strategy, even when the identification of individual modes as cut-off or cut-on is no longer possible: the acoustic energy has to be calculated summing over all modes whose amplitude is not so small as to make a negligible contribution. The simplest optimization strategy is selecting the slowest decaying mode, and choosing the impedance distribution to maximize its decay. This strategy is optimal, if this mode remains the slowest decaying, i.e., if other modes do not become dominant as a consequence of the weakening of this mode. This may be the case for a weakly non-uniform liner, if the slowest decaying mode is clearly separated from all others. If there are other modes which decay nearly as slow as the slowest, then they could become dominant if only the slowest decaying mode is subject to optimization. In the case of a strongly non-uniform liner, the modes are mixed, and thus optimization with regard to individual modes must give way to collective optimization, e.g., via the acoustic energy.

A non-uniform liner may be a passive acoustic attenuation method with some features in common with active noise reduction. Active noise reduction uses additional sound sources, with a location, amplitude and phase chosen as to reduce the noise level in certain regions: the noise level can be increased in other regions. A non-uniform liner is chosen so as to absorb more effectively

some modes, but could enhance others, so that only an assessment of the total acoustic energy can ensure an overall improvement. Compared to active noise reduction, the non-uniform liner is simpler and since it introduces no energy into the system, it runs less risk of having a negative effect in the case of poor optimization. A non-uniform liner may be less useful at: (i) low frequencies, when sound absorption is weak; (ii) high frequencies, when sound absorption is effective almost regardless of impedance distribution. The non-uniform liner is most effective at intermediate frequencies, when the impedance distribution can be "tailored" to absorb the more prominent acoustic modes. Since the non-uniform liner generates other modes, it is essential to assess correctly the benefit of the non-uniform impedance distribution. A suitable optimization criterion is, as stated before, the total acoustic energy, say in the frequency range and direction of the radiation of interest. The liner optimization may give different results depending on engine operating conditions or noise source. The compromise between different noise sources would be facilitated by an adaptive liner, whose impedance could be varied. Short of such an active–passive liner, i.e., active adaptation to passive attenuation, a fixed non-uniform liner will have to be a compromise between the optima for each noise environment it should operate in.

Acknowledgements

The present work was supported by the Silencer(r) project (G4RD-CT-2001-00500) of the Aeronautics Programme of the European Union.

References

[1] H.D. Meyer, Effect of inlet reflections on fan noise radiation, *American Institute of Aeronautics and Astronautics Journal* 34 (9) (1996) 1771–1777.
[2] S.J. Horowitz, R.K. Sigman, B.T. Zinn, An iterative method for predicting turbofan inlet acoustics, *American Institute of Aeronautics and Astronautics Journal* 20 (12) (1982) 1693–1699.
[3] S.D. Savkar, Radiation of cylindrical duct acoustic modes with flow mismatch, *Journal of Sound and Vibration* 42 (1975) 363–386.
[4] W. Koch, Radiation of sound from a two-dimensional acoustically lined duct, *Journal of Sound and Vibration* 55 (2) (1977) 255–274.
[5] S.W. Rienstra, Acoustic radiation from a semi-infinite duct in a uniform subsonic mean flow, *Journal of Sound and Vibration* 94 (2) (1984) 267–288.
[6] R. Martinez, Diffracting open-ended pipe treated as a lifting surface, *American Institute of Aeronautics and Astronautics Journal* 26 (4) (1988) 396–404.
[7] A. Snakovska, H. Idczak, B. Bogusz, Modal analysis of the acoustic field radiated from an unflanged cylindrical duct—theory and measurement, *Acustica* 82 (1996) 201–206.
[8] A. Snakowska, H. Idczak, Prediction of multitone sound radiation from a circular duct, *Acustica* 83 (1997) 955–962.
[9] P. Joseph, C.L. Morfey, Multimode radiation from an unflanged, semi-infinite circular duct, *Journal of the Acoustical Society of America* 105 (5) (1999) 2590–2600.
[10] S.T. Hocter, Exact and approximate directivity patterns of the sound radiated from cylindrical duct, *Journal of Sound and Vibration* 227 (2) (1999) 397–407.
[11] R.M. Munt, Acoustic radiation from a semi-infinite circular duct in an uniform subsonic mean flow, *Journal of Fluid Mechanics* 83 (1977) 609–640.

[12] L.M.B.C. Campos, The spectral broadening of sound by turbulent shear layers, Part 1: the transmission of sound through turbulent shear layers, *Journal of Fluid Mechanics* 89 (1978) 723–749.
[13] L.M.B.C. Campos, The spectral broadening of sound by turbulent shear layers, Part 2: the spectral broadening of sound and aircraft noise, *Journal of Fluid Mechanics* 89 (1978) 723–749.
[14] H.E. Plumblee, P.E. Doak, Duct noise radiation through a jet flow, *Journal of Sound and Vibration* 65 (4) (1979) 453–491.
[15] P.A. Nelson, C.L. Morfey, Aerodynamic sound production in low speed flow ducts, *Journal of Sound and Vibration* 79 (2) (1981) 263–289.
[16] M. Willatzen, Sound propagation in a moving fluid confined by cylindrical walls—exact series solutions for radially dependent flow profiles, *Acustica* 87 (2001) 552–559.
[17] M.S. Howe, The damping of sound by turbulent wall shear layers, *Journal of the Acoustical Society of America* 98 (1995) 1723–1730.
[18] L.M.B.C. Campos, P.G.T.A. Serrão, On the acoustics of an exponential boundary layer, *Philosophical Transactions of the Royal Society of London, Series A* 356 (1998) 2335–2378.
[19] L.M.B.C. Campos, J.M.G.S. Oliveira, M.H. Kobayashi, On sound propagation in a linear flow, *Journal of Sound and Vibration* 219 (5) (1999) 739–770.
[20] L.M.B.C. Campos, M.H. Kobayashi, On the reflection and transmission of sound in a thick shear layer, *Journal of Fluid Mechanics* 420 (2000) 1–24.
[21] A.D. Rawlins, Radiation of sound from an unflanged rigid cylindrical duct with an acoustically absorbing internal surface, *Proceedings of the Royal Society of London, Series A* 361 (1978) 65–91.
[22] K. Ogimoto, G.W. Johnston, Modal radiation impedances for semi-infinite unflanged circular ducts including flow effects, *Journal of Sound and Vibration* 62 (4) (1979) 598–605.
[23] W. Koch, W. Möhring, Eigensolutions for liners in uniform mean flow ducts, *American Institute of Aeronautics and Astronautics Journal* 21 (2) (1983) 200–213.
[24] W. Koch, Attenuation of sound in multi-element acoustically lined rectangular ducts in the absence of mean flow, *Journal of Sound and Vibration* 52 (4) (1977) 459–496.
[25] M.S. Howe, The attenuation of sound in a randomly lined duct, *Journal of Sound and Vibration* 87 (1) (1983) 83–103.
[26] S.W. Rienstra, Contributions to the theory of sound propagation in ducts with bulk-reacting lining, *Journal of the Acoustical Society of America* 77 (5) (1985) 1681–1685.
[27] D.A. Bies, C.H. Hansen, G.E. Bridges, Sound propagation in rectangular and circular cross-section ducts with flow and bulk-reacting liner, *Journal of Sound and Vibration* 146 (1) (1991) 47–80.
[28] B. Regan, J. Eaton, Modelling the influence of acoustic liner non-uniformities on duct modes, *Journal of Sound and Vibration* 219 (5) (1999) 859–879.
[29] W.R. Watson, An acoustic evaluation of circumferentially segmented duct liners, *American Institute of Aeronautics and Astronautics Journal* 22 (9) (1984) 1229–1233.
[30] C.R. Fuller, Propagation and radiation of sound from flanged circular ducts with circumferentially varying wall admittances, I: semi-infinite ducts, *Journal of Sound and Vibration* 93 (3) (1984) 321–340.
[31] C.R. Fuller, Propagation and radiation of sound from flanged circular ducts with circumferentially varying wall admittances, II: finite ducts with sources, *Journal of Sound and Vibration* 93 (3) (1984) 341–351.
[32] P.G. Vaidya, The propagation of sound in ducts lined with circumferentially non-uniform admittance of the form $\eta_0 + \eta_q \exp(\mathrm{i}q\theta)$, *Journal of Sound and Vibration* 100 (4) (1985) 463–475.
[33] L.M.B.C. Campos, J.M.G.S. Oliveira, On the acoustic modes in a cylindrical nozzle with an arbitrary impedance distribution, in preparation.
[34] C.K.W. Tam, L. Auriault, The wave modes in ducted swirling flows, *Journal of Fluid Mechanics* 371 (1998) 1–20.
[35] A.D. Pierce, *Acoustics, An Introduction to its Physical Principles*, 1st Edition, McGraw-Hill, New York, 1981.
[36] L.M.B.C. Campos, On waves in gases, Part I: Acoustics of jets, turbulence, and ducts, *Reviews of Modern Physics* 58 (1) (1986) 117–182.
[37] J.W.S. Rayleigh, *Theory of Sound*, Dover, New York, 1945.
[38] A.R. Forsyth, *Theory of Differential Functions*, Cambridge University Press, Cambridge, 1902.
[39] G.N. Watson, *Bessel Functions*, Cambridge University Press, Cambridge, 1944.

[40] H.S. Carslaw, *Theory of Fourier Series and Integrals*, Dover, New York, 1930.
[41] E.T. Whittaker, G.N. Watson, *A Course of Modern Analysis*, Cambridge University Press, Cambridge, 1927.
[42] A.E. Heins, H. Feshbach, The coupling of two acoustical ducts, *Journal of Mathematics and Physics* 26 (3) (1947) 143–155.
[43] P.H. Masterman, P.J.B. Clarricoats, Computer method of solving waveguide–iris problems, *Electronics Letters* 5 (1969) 23–25.
[44] P.H. Masterman, P.J.B. Clarricoats, Computer field-matching solution of waveguide transverse discontinuities, *Proceedings of the IEE* 118 (1) (1971) 51–63.
[45] A. Wexler, Solution of waveguide discontinuities by modal analysis, *IEEE Transactions on Microwave Theory and Techniques* MTT-15 (1967) 508–517.